Estimated strength of the Atlantic overturning circulation during the last deglaciation

Author:

Ritz, S; Stocker, T; Grimalt, J; Menviel, Laurie; Timmermann, A

Estimated strength of Atlantic overturning circulation during the last deglaciation

Supplementary information

Stefan P. Ritz[1], Thomas F. Stocker[1], Joan O. Grimalt[2], Laurie Menviel[3], and Axel Timmermann[4]

[1]Climate and Environmental Physics, Physics Institute, University of Bern, Bern, Switzerland and Oeschger Centre for Climate Change Research, University of Bern, Bern, Switzerland

[2]Department of Environmental Chemistry, Institute of Environmental Assessment and Water Research, Spanish Council for Scientific Research, Barcelona, Spain

[3]Climate Change Research Centre, Centre of Excellence, University of New South Wales, Sydney, Australia

[4]IPRC, University of Hawaii, Honolulu, USA.

1. Models

a. Bern3D

For the calculation of the coefficients of the reconstruction scheme, the Bern3D Earth System Model of intermediate complexity (B3D) is used. It consists of a frictional geostrophic ocean component with a resolution of $10°$ in longitude, a resolution between $3.2°$ and $19.2°$ in latitude (the sine of the latitude is equally spaced), and 32 depth layers[1,2]. The atmosphere consists of a two-dimensional energy and moisture balance model of the same spatial resolution as the ocean component[3,4].

In 80 simulations, a broad range of climate states is created by adding up to α Sv (1 Sv $= 10^6$ m^3 s^{-1}) freshwater to the North Atlantic from $50°$N to $70°$N to shut down the AMOC, then the same amount of freshwater is removed from the same location to induce a strong AMOC (Fig. S2). Afterwards, atmospheric CO_2 is increased from 278 ppm (parts per million) to $\beta \cdot 278$ ppm and then decreased down to $1/\beta \cdot 278$ ppm to increase and decrease air temperatures, respectively. The perturbations are applied for τ_{pert} years. A simulation is performed for every permutation of $\tau_{\mathrm{pert}} = \{1.5, 2.0, 2.5, 3.0\}$ kyr, $\alpha = \{0.15, 0.20, 0.25, 0.30\}$ Sv, and $\beta = \{1.6, 1.8, 2.0, 2.2, 2.4\}$ (Fig. S2). The reconstruction scheme coefficients are calculated for every simulation and SST location (Table S3 and Fig. S3).

b. LOVECLIM

A deglaciation simulation performed using the LOVECLIM Earth System Model of intermediate complexity (LVC)[5,6,7,8] is used to determine coefficients for the reconstruction scheme, but the simulation is also used to test the AMOC reconstruction scheme.

The ocean component of LVC consists of a free-surface primitive equation model with a horizontal resolution of $2.5°$ in longitude, $1.5°$ in latitude, and 20 depth layers. The atmospheric component is a spectral T21, three-level model based on quasi-geostrophic equations. The model is forced by the orbital coefficients, surface albedo, topography, CO_2 and freshwater[5]. The simulation covers the period from 18 to 11 ka B.P., comprises a full shutdown of the AMOC during Heinrich stadial 1 (H1) from 17.5 to 15 ka B.P., a resumption

of the AMOC during the Bølling/Allerød period from 15 to 13 ka B.P., and a second shutdown during the Younger Dryas (YD) from 13 to 12 ka B.P. Global mean air temperatures at 2 m above ground increase from 10°C at 18 ka B.P. to 13°C at 11 ka B.P. (Fig. S4). Global mean air temperature and SST time series of LVC are lowpass filtered with a cutoff period of 100 years to remove the inter-annual variability of the model.

c. NCAR CSM1.4

A freshwater forcing simulation performed using the NCAR CSM1.4 coupled atmosphere-ocean general circulation model[9,10,11] (CSM) is used to test the AMOC reconstruction scheme. This model is a comprehensive coupled climate model. The atmospheric component has a spectral truncation resolution of approximately 3.75° (T31 Grid) and 18 vertical levels. The ocean component has 25 vertical levels with a longitudinal resolution of 3.6° and a latitudinal resolution between 0.8° and 1.8°. The simulation has a duration of 605 years. At year 305, 1 Sv of freshwater is discharged into the North Atlantic for 100 years to shut down the AMOC[9] (Fig. S5). The CSM SST and global mean air temperature time series are lowpass filtered with a cutoff period of 30 years to remove inter-annual variability.

d. Model SSTs at Sediment Core Locations

When model values of SST are evaluated at sediment core locations, the SSTs of several model cells are averaged for reasons of robustness. In vertical direction, the mean value is taken over the top 80 m depth (2 cells for B3D, 5 cells for LVC, 4 cells for CSM). In horizontal direction, the 4 cells closest to the sediment core location are averaged. In the case of the CSM model, the SST of the model cell that encloses the sediment core location is averaged with all adjacent model cells in horizontal direction (9 cells if they are all ocean cells).

2. Uncertainty Calculation

The 1σ-uncertainty band of the AMOC reconstruction is calculated by Gaussian error propagation of Eq. (2). Time lags $\tau^i_{\mathrm{agescale}}$ and $\tau^{\mathrm{Tatm}}_{\mathrm{agescale}}$ are introduced to account for the age-scale uncertainty:

$$\Psi'_{\mathrm{AMOC}}(t) = \sum_{i=1}^{n} \frac{w_i}{a^i_{\mathrm{AMOC}}}[T'^i_{\mathrm{oc}}(t + \tau^i_{\mathrm{agescale}}) - a^i_{\mathrm{Tatm}}T'_{\mathrm{atm}}(t + \tau^{\mathrm{Tatm}}_{\mathrm{agescale}})]. \tag{S1}$$

The mean value of $\tau^i_{\mathrm{agescale}}$ and $\tau^{\mathrm{Tatm}}_{\mathrm{agescale}}$ is zero and for the standard deviation we estimate 500 years for the period of the last deglaciation: The age scales of the SST records are based on radiocarbon dating, and the Antarctic air temperature age scale is determined by synchronizing the methane record to the Greenland ice core record which is dated by annual layer counting for the period of the last deglaciation[12]. The uncertainties of T'^i_{oc} are given in Table S1. For the SST reconstructions that do not provide uncertainty estimates (Table S1), the maximum of the available $\Delta T'^i_{\mathrm{oc}}$ uncertainties is used (± 2.37°C). The Antarctic air temperature uncertainty is estimated to be $\Delta T'_{\mathrm{atm}} = \pm 1.5$°C. This value follows from the relative uncertainty range of the glacial-interglacial temperature amplitude of -10% to $+30\%$[13,14] and of the uncertainty range of the polar amplification of 1.7 to 2.5 which is determined from comprehensive coupled atmosphere-ocean general circulation models from the Paleoclimate Modelling Intercomparison Projects PMIP-1 and PMIP-2[15]. The uncertainties of the coefficients of the reconstruction scheme are given by the standard deviation of the coefficients of the 80 simulations performed by the B3D model. In the case of the LVC model, only one simulation is used to calculate the coefficients of the reconstruction scheme. Thus, no uncertainty can be given here.

Another factor of uncertainty is the systematic bias that may occur when SST reconstructions reflect a seasonal signal rather than an annual mean signal[16,17]. Leduc et al.[16] have compared a global compilation of SST time series records from the Holocene and detected contrasting, sometimes divergent, SST trends

throughout the Holocene proxy records of marine sediment cores from the same region, which is hypothesized to be due to the different trends of the Holocene summer and winter solar insolation. This factor of uncertainty can be minimized by only using SST reconstructions that truly represent annual-mean temperatures. This can potentially be achieved by preferring Mg/Ca-derived SST time series over $U_{37}^{K'}$-derived SSTs. However, due to the already small number of suitable Atlantic SST records of sufficient time resolution, we continue to use all proxies for the time being.

3. Additional Tables and Figures

Here supplementary tables and figures referenced in the main text are given. Tables S1 and S2 and Fig. S1 give information on the SST sediment core reconstructions used for the AMOC reconstruction. Tables S3 and S4 list the reconstruction scheme coefficients based on the B3D simulations and the LVC deglaciation simulation, respectively. Table S5 lists the weights that are assigned to the SST time series for the AMOC reconstructions.

Figure S6 illustrates that the AMOC peak between 15 and 14 ka B.P. is better captured when an additional SST time series from the central North Atlantic is incorporated into the hindcast.

Figure S7 illustrates the difference in the linear combination of Eq. (1) when global, Antarctic, or Greenland air temperatures are used for the linear combination.

Figure S8 illustrates that inaccurate coefficients a_{Tatm}^{i} may lead to a trend in Ψ'_{AMOC} in the case where $T_{\mathrm{oc}}^{\prime i}$ and T'_{atm} change simultaneously such as during a deglaciation. An extreme situation of a hindcast of the LVC deglaciation simulation is shown where all a_{Tatm}^{i} are set to $0\,\mathrm{K\,K^{-1}}$.

TABLE S1. SST reconstructions from various Atlantic sites that are used for the last deglaciation AMOC reconstruction. The data sets span at least 19 kyr and have an average resolution better than 500 yr. The location of the sites is indicated on the map in Fig. S1. For data sets that span longer periods than the last 25 kyr, the average resolution of the last 25 kyr is listed. $\Delta T'_{\mathrm{oc}}$ is the temperature reproducibility uncertainty. Waelbroeck et al.[18] give individual uncertainties for every data point. Here, the mean value is used. Proxies used for the temperature reconstruction are the revised analogue method (RAM), the Mg/Ca ratio from shells of planktonic foraminifera, and the alkenone unsaturation index $U_{37}^{K'}$.

#	Core	Lat (°)	Lon (°)	time span (ka B.P.)	avg res (yr)	$\Delta T'_{\mathrm{oc}}$ (°C)	Proxy	Reference
1	CH 69–K09	41.7	−47.5	19 − 1	156	±2.37	RAM	Waelbroeck et al.[18]
2	NA 87–22	55.5	−14.7	23 − 1	204	±0.90	RAM	Waelbroeck et al.[18]
3	SU 81–18	37.8	−10.2	20 − 0	480	±0.82	RAM	Waelbroeck et al.[18]
4	PL07–39PC	10.7	−64.9	25 − 0	133	±0.7	Mg/Ca	Lea et al.[19]
5	GeoB 3129–1 GeoB 3911–3	−4.6	−36.6	21 − 0	125	±1.0	Mg/Ca	Weldeab et al.[20]
6	MD03–2707	2.5	9.4	155 − 0	67	±1.2	Mg/Ca	Weldeab et al.[21]
7	GeoB 4905–4	2.5	9.4	22 − 0	199	±1.0	Mg/Ca	Weldeab et al.[22]
8	ODP 1084B	−25.5	13.0	21 − 0	96	±0.6	Mg/Ca	Farmer et al.[23]
9	MD01–2444	37.8	−10.2	420 − 0	128	±0.5	$U_{37}^{K'}$	Martrat et al.[24]
10	SU81-18 MD95–2042	37.8	−10.2	110 − 0	306	±0.4	$U_{37}^{K'}$	Bard[25], Bard et al.[26]
11	MD03–2699	39.0	−10.7	23 − 1	152	±0.5	$U_{37}^{K'}$	Rodrigues et al.[27]
12	M39–008	36.4	−7.1	21 − 1	184	±0.5	$U_{37}^{K'}$	Cacho et al.[28]
13	ODP 658C	20.8	−18.6	84 − 0	201	−	$U_{37}^{K'}$	Zhao et al.[29]
14	GeoB 1023–5	−17.2	11.0	21 − 0	112	±0.1	$U_{37}^{K'}$	Kim et al.[30]

TABLE S2. Links to the SST and air temperature data.

#	Reference	Link
–	Jouzel et al.[14]	ftp://ftp.ncdc.noaa.gov/pub/data/paleo/icecore/antarctica/epica_domec/edc3deuttemp2007.txt
1–3	Waelbroeck et al.[18]	personal communication
4	Lea et al.[19]	ftp://ftp.ncdc.noaa.gov/pub/data/paleo/paleocean/sediment_files/complete/pl07-39p-tab.txt
5	Weldeab et al.[20]	ftp://ftp.ncdc.noaa.gov/pub/data/paleo/contributions_by_author/weldeab2006/weldeab2006.txt
6	Weldeab et al.[21]	ftp://ftp.ncdc.noaa.gov/pub/data/paleo/paleocean/sediment_files/complete/md3-2707-tab.txt
7	Weldeab et al.[22]	personal communication
8	Farmer et al.[23]	ftp://ftp.ncdc.noaa.gov/pub/data/paleo/paleocean/sediment_files/complete/odp1084b-tab.txt
9	Martrat et al.[24]	http://doi.pangaea.de/10.1594/PANGAEA.771891
10	Bard[25], Bard et al.[26]	ftp://ftp.ncdc.noaa.gov/pub/data/paleo/paleocean/sediment_files/complete/ibermarg-tab.txt
11	Rodrigues et al.[27]	http://doi.pangaea.de/10.1594/PANGAEA.761812
12	Cacho et al.[28]	ftp://ftp.ncdc.noaa.gov/pub/data/paleo/contributions_by_author/cacho2001/cacho2001.txt
13	Zhao et al.[29]	ftp://ftp.ncdc.noaa.gov/pub/data/paleo/paleocean/sediment_files/complete/odp658cz-tab.txt
14	Kim et al.[30]	ftp://ftp.ncdc.noaa.gov/pub/data/paleo/paleocean/sediment_files/complete/gb1023-5-tab.txt

TABLE S3. Reconstruction scheme coefficients at the SST sediment core locations of Table S1 calculated from 80 Bern3D model simulations (Fig. S2). Also listed are the correlations between ocean temperature at the particular location and air temperature (R_{Tatm}), and between ocean temperature and the least squares fit (R_{fit}) averaged over the 80 simulations.

#	a_{Tatm} (K K^{-1})	a_{AMOC} (K Sv^{-1})	R_{Tatm}	R_{fit}
1	0.72 ± 0.02	0.099 ± 0.007	0.73	0.97
2	1.01 ± 0.07	0.33 ± 0.04	0.34	0.93
3/9/10/11/12	0.88 ± 0.04	0.19 ± 0.02	0.52	0.92
4	0.784 ± 0.008	0.018 ± 0.006	0.97	0.98
5	0.70 ± 0.01	-0.035 ± 0.007	0.96	0.99
6/7	0.713 ± 0.008	-0.004 ± 0.004	0.97	0.97
8	0.60 ± 0.02	-0.051 ± 0.010	0.88	0.97
13	0.86 ± 0.03	0.10 ± 0.03	0.71	0.90
14	0.64 ± 0.03	-0.11 ± 0.02	0.75	0.96

Table S4. Reconstruction scheme coefficients at the SST sediment core locations of Table S1 calculated based on the LOVECLIM deglaciation simulation. Also listed are the correlations between ocean temperature at the particular location and air temperature (R_{Tatm}), and between ocean temperature and the least squares fit (R_{fit}).

#	a_{Tatm} $(\mathrm{K\,K^{-1}})$	a_{AMOC} $(\mathrm{K\,Sv^{-1}})$	R_{Tatm}	R_{fit}
1	0.94	−0.022	0.84	0.85
2	1.23	0.27	0.84	0.99
3/9/10	0.83	0.16	0.86	0.98
4	0.20	−0.031	0.29	0.75
5	0.24	−0.0051	0.77	0.77
6/7	0.45	−0.034	0.72	0.84
8	0.37	−0.086	0.03	0.96
11	0.89	0.19	0.85	0.99
12	0.90	0.15	0.88	0.99
13	0.41	0.064	0.88	0.99
14	0.28	−0.057	0.12	0.93

Table S5. The weights w_i that are assigned to the SST time series for the two AMOC reconstructions. The weights follow from the least squares solution (Eq. 2). The sum of the weights is equal to 1.

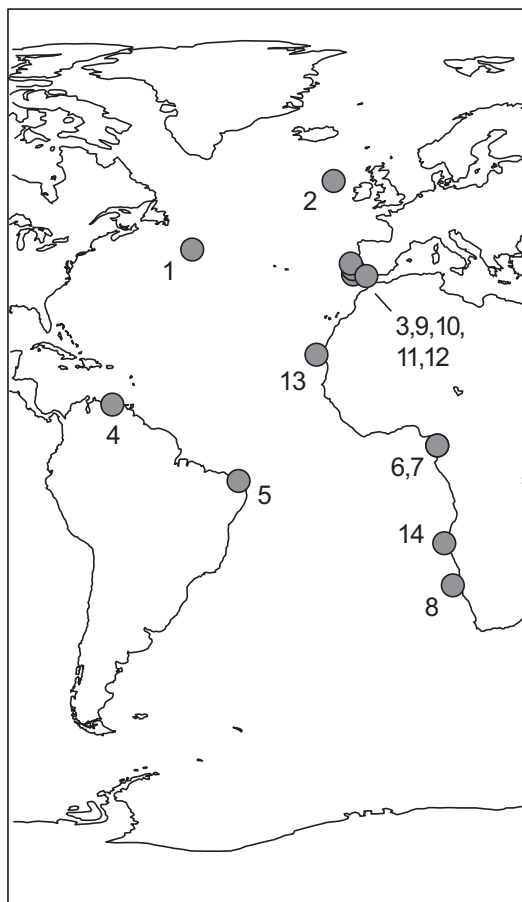| #	LOVECLIM	Bern3D
1	0.002	0.031
2	0.325	0.337
3	0.111	0.110
4	0.004	0.001
5	0.000	0.004
6	0.005	0.000
7	0.005	0.000
8	0.034	0.008
9	0.111	0.110
10	0.111	0.110
11	0.161	0.110
12	0.097	0.110
13	0.019	0.034
14	0.015	0.036

Fig. S1. Locations of sea-surface temperature time series reconstructions used for the reconstruction of the AMOC anomalies of the last deglaciation. The index numbers correspond to the numbers in Table S1 where the SST reconstructions are listed.
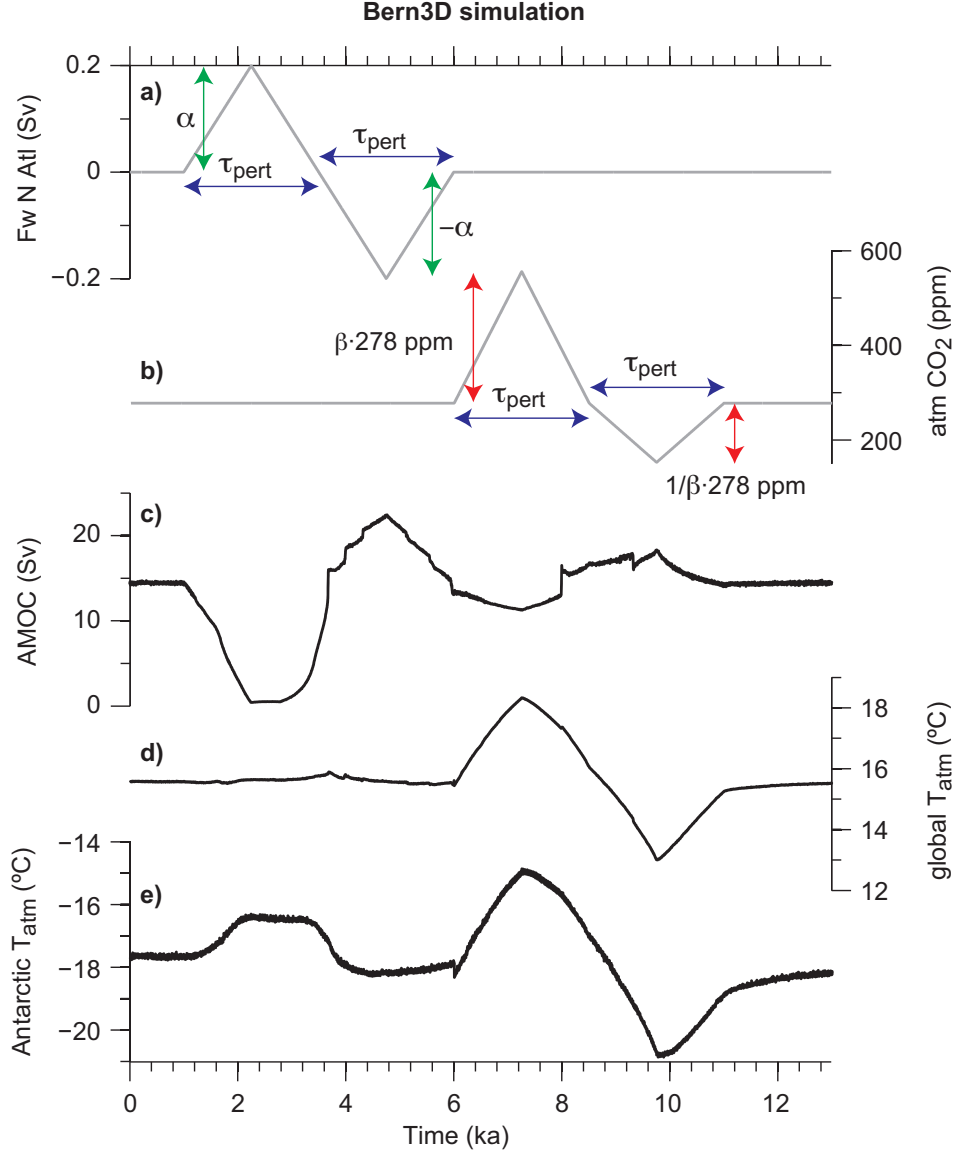
FIG. S2. Forcings (gray) and responses (black) of the Bern3D model to determine the coefficients of Eq. (1). In 80 simulations, a broad range of climate states is created by a) adding and removing up to α Sv (1 Sv = 10^6 m^3 s^{-1}) freshwater (Fw) from the North Atlantic from 50°N to 70°N, and b) by increasing atmospheric CO_2 from 278 ppm to $\beta \cdot 278$ ppm and then decreasing CO_2 down to $1/\beta \cdot 278$ ppm. The perturbations are applied for τ_{pert} years. A simulation is performed for every permutation of $\tau_{\text{pert}} = \{1.5, 2.0, 2.5, 3.0\}$ kyr, $\alpha = \{0.15, 0.20, 0.25, 0.30\}$ Sv, and $\beta = \{1.6, 1.8, 2.0, 2.2, 2.4\}$. The result is c) a shutdown of the AMOC followed by an AMOC state substantially stronger than in the standard case, and d-e) changes of global mean and Antarctic air temperatures of several degrees. The figure shows results from one of the 80 simulations.
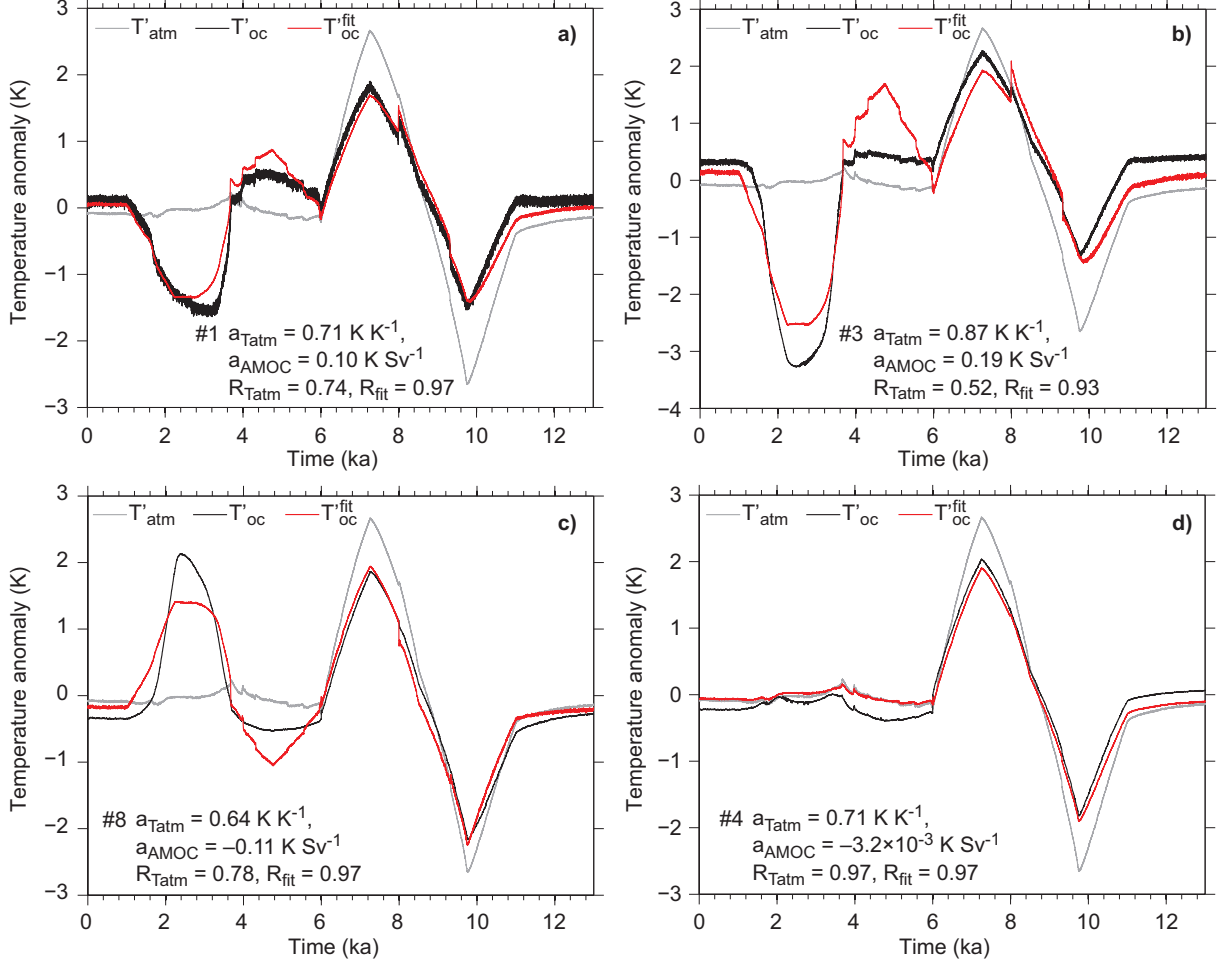
FIG. S3. Examples of the determination of the coefficients of Eq. (4) at the sediment core locations 1, 3, 4, and 8 (see Table S1 and Fig. S1) by using one of the model simulations described in Fig. S2. Panel a: core location 1 (Northwest Atlantic); panel b: core location 3 (Iberian Margin); panel c: core location 8 (Southeast Atlantic); panel d: core location 4 (Cariaco Basin). Gray line: global mean air temperature anomaly. Black line: ocean temperature anomaly at the sediment core location. Red line: least squares fit of the ocean temperature anomaly according to Eq. (4). The reconstruction scheme coefficients and the correlations between ocean temperature and air temperature (R_{Tatm}), and between ocean temperature and the least squares fit (R_{fit}) are given in the figure. The locations of examples a-c are sensitive to the AMOC, as indicated by the difference of R_{Tatm} and R_{fit}. The location of example d is not sensitive to AMOC changes.
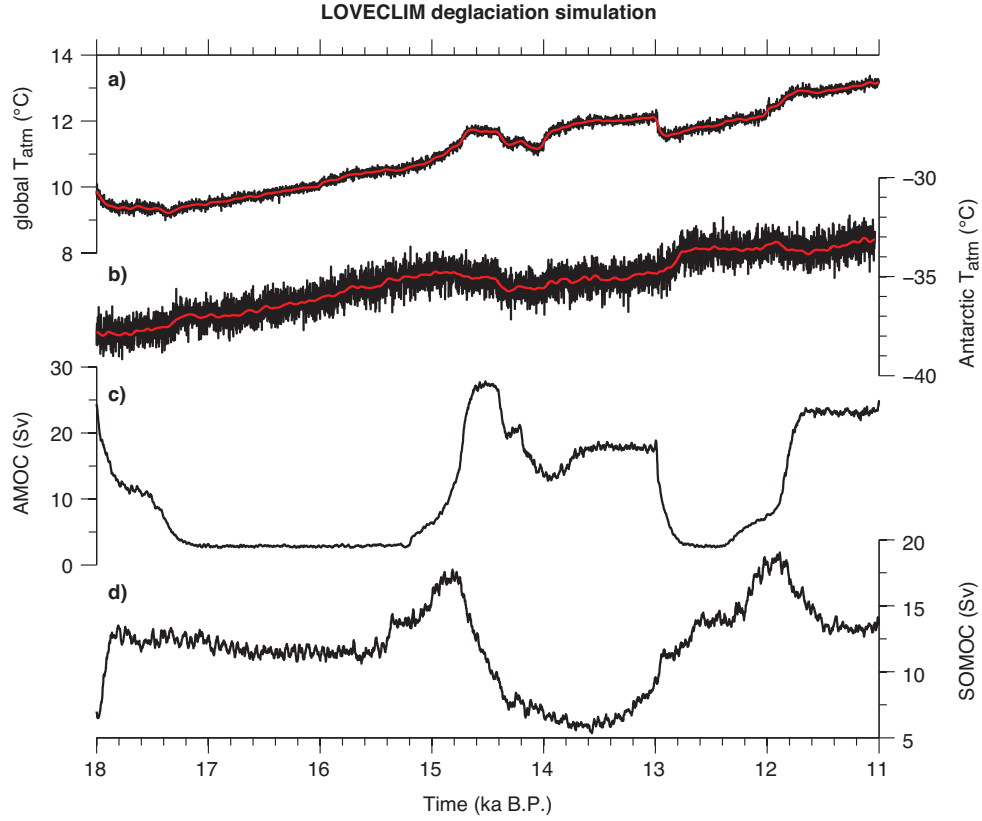
8

FIG. S4. LOVECLIM simulation of the last deglaciation[5]. a) Global mean surface air temperature. b) Antarctic mean surface air temperature. c) AMOC strength. d) Southern Ocean meridional overturning circulation (SOMOC) strength. Red lines are splines with a cutoff period of 100 yr to remove inter-annual variability.
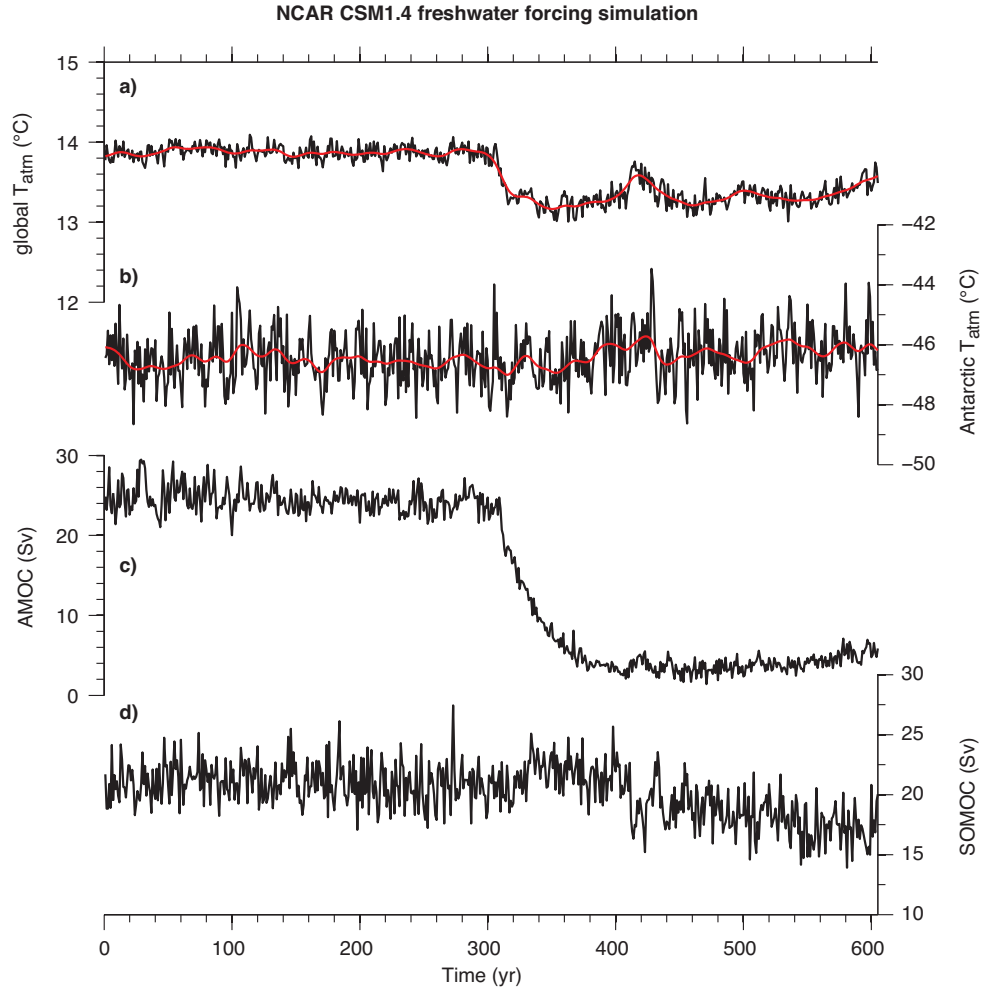
FIG. S5. NCAR CSM1.4 freshwater forcing simulation [9]. a) Global mean surface air temperature. b) Antarctic surface air temperature at the location of the Dome C ice core. c) AMOC strength. d) SOMOC strength. Red lines are splines with a cutoff period of 30 yr to remove inter-annual variability.
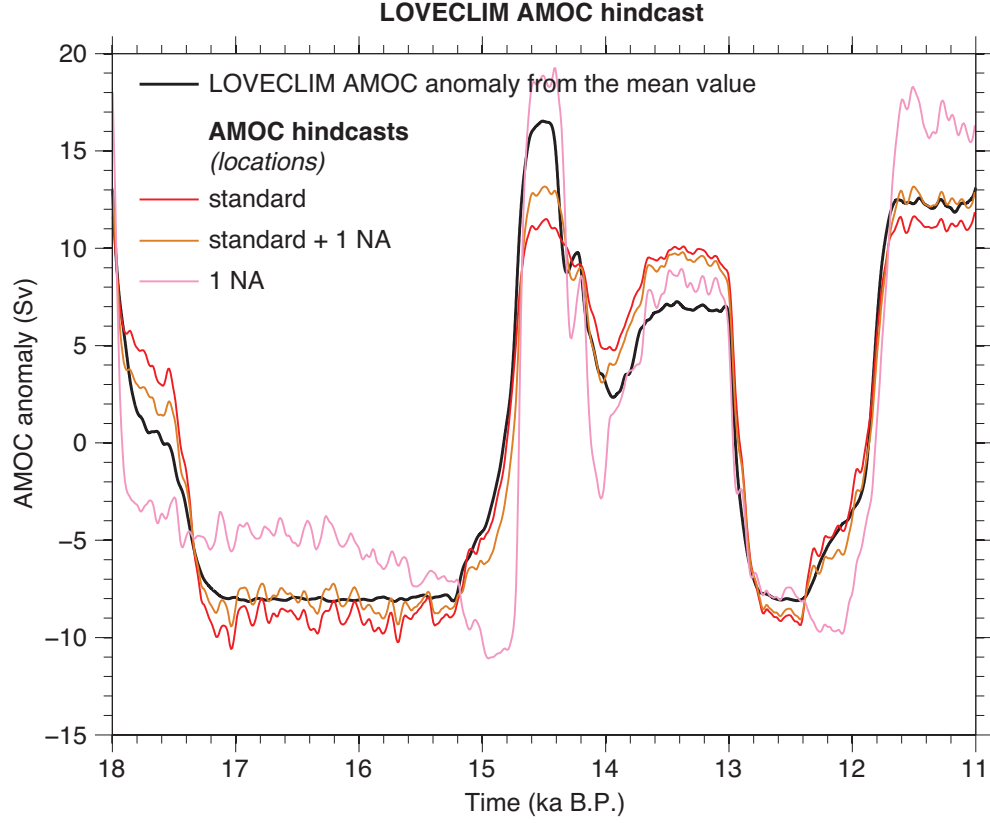
10

LOVECLIM AMOC hindcast

Fig. S6. Hindcasts of the LOVECLIM deglaciation simulation based on coefficients determined from the LOVECLIM simulation. The hindcast is given as anomaly from the time series mean value. Red line: Hindcast when the 14 SST time series of Table S1 are used (as in Fig. 2a). In this hindcast, the AMOC peak between 15 and 14 ka B.P. is not captured. The peak is somewhat better captured when an additional SST time series from the central North Atlantic (NA, at 50°N, 35°W) is incorporated into the hindcast (orange line). Pink line: Hindcast when only the central North Atlantic SST time series is used. This hindcast reproduces the AMOC peak between 15 and 14 ka B.P. Unfortunately, to date there is no SST reconstruction at this site.
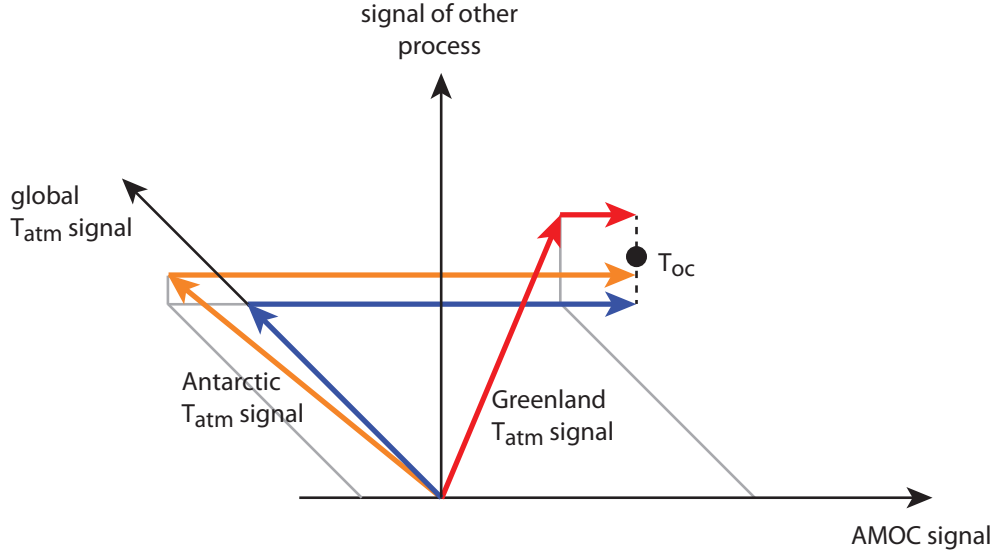
FIG. S7. The ocean temperature time series at any Atlantic SST location can be described as a linear combination of global mean atmospheric temperature time series (which is mostly independent of AMOC changes), the AMOC time series, and time series of other quantities that affect ocean temperature (blue arrows). Here it is assumed that these other quantities have little influence on Atlantic SST on centennial to glacial-interglacial timescales. The quantities of the linear combination do not necessarily need to be orthogonal. The ocean temperature could also be a linear combination of Greenland air temperature and AMOC time series (red arrows). However, in this case the AMOC coefficient (a_{AMOC}) of a northern hemisphere SST location will be small. And the smaller the AMOC coefficient, the more uncertain the reconstruction may become. Because to this date there is no direct paleoclimate proxy of global mean air temperature, Antarctic air temperatures could be used (orange arrows). Because of the bipolar seesaw[31], the Antarctic air temperature signal tends to be anticorrelated to the AMOC signal. Hence, a_{AMOC} will tend to be more positive in the northern hemisphere (and less negative in the southern hemisphere) than when global mean air temperatures are used.
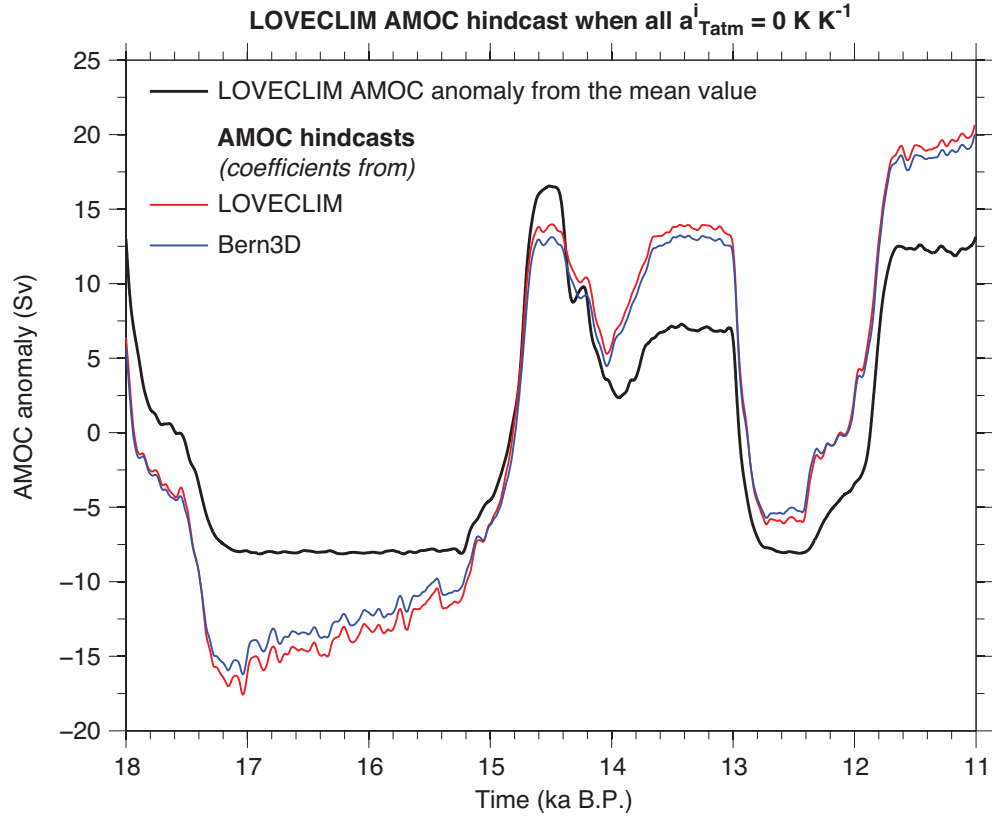
FIG. S8. Hindcasts of the LOVECLIM deglaciation simulation when all a^i_{Tatm} are set to $0\ \mathrm{K\,K}^{-1}$. This figure illustrates the trend in Ψ'_{AMOC} that may arise in the case of inaccurate a^i_{Tatm}. Black line: LOVECLIM AMOC anomaly. Red line: AMOC hindcast calculated from coefficients determined by the LOVECLIM simulation (with $a^i_{\mathrm{Tatm}} = 0\ \mathrm{K\,K}^{-1}$). Blue line: Hindcast from coefficients determined by Bern3D (with $a^i_{\mathrm{Tatm}} = 0\ \mathrm{K\,K}^{-1}$).

REFERENCES

1. Edwards, N. R. & Marsh, R. Uncertainties due to transport-parameter sensitivity in an efficient 3-D ocean-climate model. *Climate Dynamics* **24**, 415–433 (2005).

2. Müller, S. A., Joos, F., Edwards, N. R. & Stocker, T. F. Water mass distribution and ventilation time scales in a cost-efficient, three-dimensional ocean model. *Journal of Climate* **19**, 5479–5499 (2006).

3. Ritz, S. P., Stocker, T. F. & Joos, F. A coupled dynamical ocean – energy balance atmosphere model for paleoclimate studies. *Journal of Climate* **24**, 349–375 (2011).

4. Ritz, S. P., Stocker, T. F. & Severinghaus, J. P. Noble gases as proxies of mean ocean temperature: sensitivity studies using a climate model of reduced complexity. *Quaternary Science Reviews* **30**, 3728–3741 (2011).

5. Menviel, L., Timmermann, A., Elison Timm, O. & Mouchet, A. Deconstructing the Last Glacial termination: the role of millennial and orbital-scale forcings. *Quaternary Science Reviews* **30**, 1155–1172 (2011).

6. Driesschaert, E. *et al.* Modeling the influence of Greenland ice sheet melting on the Atlantic meridional overturning circulation during the next millennia. *Geophysical Research Letters* **34** (2007).

7. Goosse, H., Driesschaert, E., Fichefet, T. & Loutre, M.-F. Information on the early Holocene climate constrains the summer sea ice projections for the 21st century. *Climate of the Past* **3**, 683–692 (2007).

8. Goosse, H. *et al.* Description of the Earth system model of intermediate complexity LOVECLIM version 1.2. *Geoscientific Model Development* **3**, 603–633 (2010).

9. Bozbiyik, A., Steinacher, M., Joos, F., Stocker, T. F. & Menviel, L. Fingerprints of changes in the terrestrial carbon cycle in response to large reorganizations in ocean circulation. *Climate of the Past* **7**, 319–338 (2011).

10. Fung, I. Y., Doney, S. C., Lindsay, K. & John, J. Evolution of carbon sinks in a changing climate. *PNAS* **102**, 11201–11206 (2005).

11. Doney, S. C., Lindsay, K., Fung, I. & John, J. Natural variability in a stable, 1000-yr global coupled climate–carbon cycle simulation. *Journal of Climate* **19**, 3033–3054 (2006).

12. Parrenin, F. *et al.* The EDC3 chronology for the EPICA Dome C ice core. *Climate of the Past* **3**, 485–497 (2007).

13. Jouzel, J. *et al.* Magnitude of isotope/temperature scaling for interpretation of central Antarctic ice cores. *Journal of Geophysical Research* **108**, D12 (2003).

14. Jouzel, J. *et al.* Orbital and millennial Antarctic climate variability over the past 800,000 years. *Science* **317**, 793–796 (2007).

15. Masson-Delmotte, V. *et al.* EPICA Dome C record of glacial and interglacial intensities. *Quaternary Science Reviews* **29**, 113–128 (2010).

16. Leduc, G., Schneider, R., Kim, J.-H. & Lohmann, G. Holocene and Eemian sea surface temperature trends as revealed by alkenone and Mg/Ca paleothermometry. *Quaternary Science Reviews* **29**, 989–1004 (2010).

17. Schneider, B., Leduc, G. & Park, W. Disentangling seasonal signals in Holocene climate trends by satellite-model-proxy integration. *Paleoceanography* **25**, PA4217 (2010).

18. Waelbroeck, C. *et al.* The timing of the last deglaciation in North Atlantic climate records. *Nature* **412**, 724–727 (2001).

19. Lea, D. W., Pak, D. K., Peterson, L. C. & Hughen, K. A. Synchroneity of tropical and high-latitude Atlantic temperatures over the last glacial termination. *Science* **301**, 1361–1364 (2003).

20. Weldeab, S., Schneider, R. R. & Kölling, M. Deglacial sea surface temperature and salinity increase in the western tropical Atlantic in synchrony with high latitude climate instabilities. *Earth and Planetary Science Letters* **241**, 699–706 (2006).

21. Weldeab, S., Lea, D. W., Schneider, R. R. & Andersen, N. 155,000 years of West African Monsoon and Ocean Thermal Evolution. *Science* **316**, 1303–1307 (2007a).

22. Weldeab, S., Schneider, R. R. & Müller, P. Comparison of Mg/Ca- and alkenone-based sea surface temperature estimates in the fresh water-influenced Gulf of Guinea, eastern equatorial Atlantic. *Geochemistry Geophysics Geosystems* **8**, Q05P22 (2007b).

23. Farmer, E. C., deMenocal, P. B. & Marchitto, T. M. Holocene and deglacial ocean temperature variability in the Benguela upwelling region: Implications for low-latitude atmospheric circulation. *Paleoceanography* **20**, PA2018 (2005).

24. Martrat, B. *et al.* Four climate cycles of recurring deep and surface water destabilizations on the Iberian Margin. *Science* **317**, 502–507 (2007).

25. Bard, E. Climate shock: abrupt changes over millennial time scales. *Physics Today* **55**, 32–38 (2002).

26. Bard, E., Ménot-Combes, G. & Rostek, F. Present status of radiocarbon calibration and comparison records based on polynesian corals and Iberian Margin sediments. *Radiocarbon* **46**, 1189–1203 (2004).

27. Rodrigues, T., Grimalt, J. O., Abrantes, F., Naughton, F. & Flores, J.-A. The last glacial–interglacial transition (LGIT) in the western mid-latitudes of the North Atlantic: Abrupt sea surface temperature change and sea level implications. *Quaternary Science Reviews* **29**, 1853 – 1862 (2010).

28. Cacho, I. *et al.* Variability of the western Mediterranean Sea surface temperature during the last 25,000 years and its connection with the Northern Hemisphere climatic changes. *Paleoceanography* **16**, 40–52 (2001).

29. Zhao, M., Beveridge, N. A. S., Shackleton, N. J., Sarnthein, M. & Eglinton, G. Molecular stratigraphy of cores off northwest Africa – sea-surface temperature history over the last 80 ka. *Paleoceanography* **10**, 661–675 (1995).

30. Kim, J.-H., Schneider, R. R., Müller, P. J. & Wefer, G. Interhemispheric comparison of deglacial sea-surface temperature patterns in atlantic eastern boundary currents. *Earth and Planetary Science Letters* **194**, 383–393 (2002).

31. Stocker, T. F. & Johnson, S. J. A minimum thermodynamic model for the bipolar seesaw. *Paleoceanography* **18**, 1087 (2003).